Pergamon

Int. J. Heat Mass Transfer. Vol. 39, No. 17, pp. 3733–3748, 1996

0017–9310/96 $15.00 + 0.00

PII: S0017–9310(96)00015–4

Theory of transient experimental techniques for surface heat transfer

JAN TALER

Cracow University of Technology, Department of Mechanical Engineering, PL-31-155 Kraków, ul. Warszawska 24, Poland

(*Received* 27 *October* 1994 *and in final form* 9 *May* 1995)

Abstract—The paper describes the unified mathematical procedures of transient methods for measuring surface heat transfer rates. Three heat flux gauges are discussed: thin film, thick-wall gauges placed on semi-infinite substrates and thin-skin calorimeters. The aim of this paper is to present a method for a simple and accurate determination of the time-varying heat transfer coefficient (or heat flux) given an accurate temperature history of the body at a selected point beneath the surface. The interior temperature measurements are converted into local instantaneous heat transfer coefficients by solving the inverse heat conduction problem for the gauge. The effect of the inaccuracies in the measurement of the interior temperature was eliminated by cubic spline smoothing or digital filtering of the raw interior temperature data prior to using it in the inverse heat conduction analyses. General case closed form equations for instantaneous surface heat flux, or heat transfer coefficient, are developed. Copyright © 1996 Elsevier Science Ltd.

INTRODUCTION

Most heat transfer measurements consist of monitoring the temperature of a body at selected points and then relating that temperature history to the one of heat transfer rate. In a general case, the temperatures measured are related in a complex way to the heat transfer coefficients and hence, measurements are usually made with geometries such that only one spatial coordinate needs to be considered. The usual quantities of interest are the local heat flux $q_s(t)$, and the convective heat transfer $h(t)$. If the radiation can be neglected, the local heat transfer coefficient can be easily related to the heat flux

$$h = \frac{q_s}{T_\infty - T_s}, \tag{1}$$

where T_s represents the material surface temperature and T_∞ is the fluid temperature far away from the wall. The devices for measuring heat transfer between a flowing fluid and a solid surface can be categorized as gauges: (1) semi-infinite one-dimensional gauges, (2) thin-skin calorimeter gauges, and (3) thick-wall gauges.

The first method records instantaneous surface temperature from which instantaneous heat flux rates are deduced using the heat conduction solution for the semi-infinite substrate [Fig. 1(a)].

The surface heat flux is obtained by using the one-dimensional, semi-infinite medium solution for a step change in surface temperature [1] and applying Duhamel's superposition integral to give

$$q(t) = \sqrt{\frac{\rho c k}{\pi}} \int_0^t \frac{1}{\sqrt{t-\Theta}} \frac{\mathrm{d}f(\Theta)}{d\Theta} \mathrm{d}\Theta, \tag{2}$$

where $f(t)$ is the measured surface temperature history. Such a one-dimensional heat flow can also be achieved by having the conducting material in the form of a rod or a strip that is well insulated from the surrounding model.

One-dimensional gauges employing surface thermocouples on such conducting rods fall into this category because they can be considered semi-infinite as the thermal penetration distance during experimental run-times is small compared to the linear dimension of the gauge [2–11].

The most popular measurement method for the surface temperature is the thin-film metal resistance layers (such as palladium on MACOR or platinum on quartz) [3–5, 7] or a surface thermocouples (such as coaxial or eroding thermocouples) [8, 11]. The surface temperature can also be determined from the calibrated liquid-crystal colour [9, 10]. The thin-skin method is one of the oldest, simplest and most effective methods of obtaining transient heat flux [12–16].

The calorimetric element is very thin [Fig. 1(b)], so the rate of rise of the rear surface temperature, which is usually monitored, is equal to the rate of rise of the mean temperature. The expression used to obtain transient heat flux data is given by

$$q(t) = \rho c E \frac{\mathrm{d}f}{\mathrm{d}t}, \tag{3}$$

where $f(t)$ is the back surface temperature history. Equation (3) assumes no heat losses at the back surface and a negligible temperature drop across the calorimeter wall.

In the case of thick-wall gauges [Fig. 1(c)], the heat received by the gauge is largely stored within the gauge

NOMENCLATURE

a	time at which heat flux is maximal [s]
$A_0, \ldots, A_m$	coefficients of temperature-time polynomials
Bi	Biot number, $Bi = hx/k$
c	specific heat [J kg^{-1} K^{-1}]
$C_{1,j}, \ldots, C_{4,j}$	coefficients (derivatives) of the piecewise cubic function
D	heating duration [s]
e	maximal temperature error [K]
E	thermocouple depth below heated or cooled surface [m]
f	measured temperature at an interior point [°C]
h	heat transfer coefficient [W m^{-2} K^{-1}]
J	total number of the data points
k	thermal conductivity [W m^{-1} K^{-1}]
N	number of data points used in digital filtering
q	heat flux [W m^{-2}]
S	least squares function [K^2]
S_t	time scaling factor
t	time [s]
T	temperature [°C]
T_0	initial temperature distributions
w_i	weighting factor
x	spatial coordinate [m]
Y	smoothed value of measured temperature at an interior point [°C].

Greek symbols

α	thermal diffusivity, $\alpha = k/c\rho$ [m^2 s^{-1}]
Δt	time step [s]
ε_i	random variable of uniform distribution with values in the range $[-1, 1]$
η	dimensionless parameter, $\eta = h^2 t/c\rho k$
Θ	dummy time variable
λ	smoothing (regularization) parameter
ξ	dimensionless parameter, $\xi = x/2\sqrt{\alpha t}$
ρ	density [kg m^{-3}]
σ	root mean square norm
τ	scaled time.

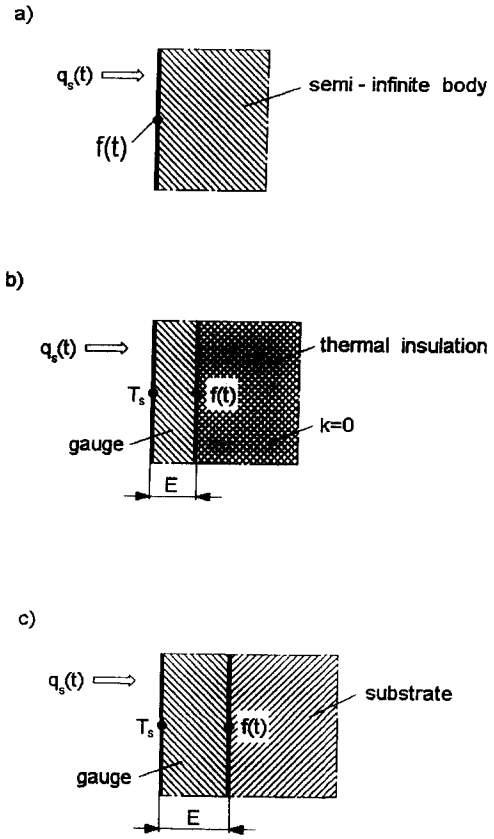

Fig. 1. Basic geometries of gauges used in heat transfer measurements: (a) semi-infinite one-dimensional gauge; (b) thin-wall (calorimeter) gauge; (c) thick-wall gauge.

while only a small portion is transferred to the substrate.

In this case the measured temperature is related in a more complex way to surface heat flux than that for thin-skin calorimeters.

ANALYSIS

The physical model that may be applied to both the semi-infinite and calorimeter gauge is that of a uniform slab on a semi-infinite substrate composed of different material.

The instantaneous surface temperature $f(t)$ of the substrate is measured at $x = E$. The problem is to calculate the front surface temperature and the heat flux at $x = 0$ given the measured temperature at point $x = E$.

The problem can be subdivided into two separate problems, one of which is a direct problem, as shown in Fig. 2. The semi-infinite body from $x = E$ to $x \to \infty$ can be analysed as a direct problem because the boundary conditions at both boundaries are known [$T_2(E, t) = f(t)$ at $x = E$, $\partial T_2/\partial x = 0$ and $T_2 = T_0$ at $x \to \infty$]. When substrate thermal properties are treated as constant, the heat flux q_E passing through surface $x = E$ is calculated by converting the measured temperature history to heat transfer rate by using Duhamel's Theorem (2).

The same heat flux q_E must leave body 1 ($0 \leqslant x \leqslant E$). Two conditions (temperature and heat flux) are prescribed at $x = E$ in body 1 and none at

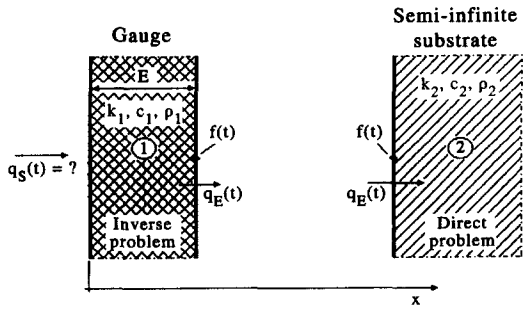

Fig. 2. Subdivisions of an inverse heat conduction problem into inverse and direct problems.

$x = 0$. The surface temperature $T_S = T_1(0, t)$ and heat flux $q_S = -k_1 \partial T_1/\partial x\,|_{x=0}$ histories of body 1 must be determined from conditions at location $x = E$. Such a problem is referred to as an inverse problem.

The general solution of the inverse problem was independently given by Stefan [17], Burggraf [18] and Langford [19]

$$T_1(x,t) = y(t) + \sum_{n=1}^{\infty} \frac{1}{(2n)!} \frac{(E-x)^{2n}}{\alpha_1^n} \frac{\mathrm{d}^n y}{\mathrm{d}t^n} + \frac{(E-x)}{k_1}\left[q_E(t) + \sum_{n=1}^{\infty} \frac{1}{(2n+1)!} \frac{(E-x)^{2n}}{\alpha_1^n} \frac{\mathrm{d}^n q_E}{\mathrm{d}t^n}\right] \quad (4)$$

$$q_s(t) = -k_1 \left.\frac{\partial T_1}{\partial x}\right|_{x=0} = q_E(t) + k_1 \sum_{n=1}^{\infty} \frac{E^{2n-1}}{(2n-1)!} \frac{1}{\alpha_1^n} \frac{\mathrm{d}^n y}{\mathrm{d}t^n} + \sum_{n=1}^{\infty} \frac{E^{2n}}{(2n)!} \frac{\mathrm{d}^n q_E}{\mathrm{d}t^n} \frac{1}{\alpha_1^n}. \quad (5)$$

The solution requires that finite order derivatives of the measured temperature $y(t)$ and calculated heat flux $q_E(t)$ at interior location $x = E$ must exist. The method is stable for any time step, provided $\mathrm{d}^n y/\mathrm{d}t^n$ and $\mathrm{d}^n q_E/\mathrm{d}t^n$ are bounded.

Unwanted oscillations (oscillatory instability) can be produced in the calculated surface temperature or heat flux if the time derivatives are not calculated with sufficient accuracy.

The above series converge quite rapidly, so that only the first few time derivatives need to be considered.

Truncating equations (4) and (5) after the third or second derivative yields approximate solutions of acceptable accuracy.

In a heat-conduction body, variations in the surface conditions are always damped at the interior points. In the inverse heat conduction problems, the surface temperature and heat flux histories are obtained from the damped temperature data taken at a subsurface location. Therefore, one cannot hope to find the higher frequency components of the boundary conditions using only interior temperature measurements, especially when the temperature sensor is located far from the surface.

To determine rapid variations in the surface conditions, the temperature sensor should be placed as close to the surface as possible.

HEAT FLUX TRANSFERRED TO SUBSTRATE MATERIALS

The temperature measurements at $x = E$ are made at discrete times: $t_1, t_2, \ldots, t_M$ or in general at time t_i at which the temperature measurement is denoted f_i. If the interface temperature between successive times is assumed to vary linearly with time (Fig. 3), equation (2) can be integrated analytically to give [2]

$$q_E(t_{M+1}) = -k_2 \left.\frac{\partial T_2}{\partial x}\right|_{x=E} = -k_1 \left.\frac{\partial T_1}{\partial x}\right|_{x=E} = 2\sqrt{\frac{k_2\rho_2 c_2}{\pi}} \sum_{i=1}^{M} \frac{f_{i+1} - f_i}{\sqrt{t_{M+1} - t_{i+1}} + \sqrt{t_{M+1} - t_i}}. \quad (6)$$

Polynomial regression data fitting technique can also be applied to smooth the surface temperature–time response

$$y(t) = A_0 + A_1 t + A_2 t^2 + , \cdots , + A_m t^m = \sum_{i=0}^{m} A_i t^i. \quad (7)$$

Substituting of the polynomial approximation (7) into equation (2) and its integrating yields [20]

$$q_E(t) = 2\sqrt{\frac{c_2\rho_2 k_2}{\pi}} \left\{ A_1 \sqrt{t} + \sum_{i=2}^{m} i A_i t^{(2i-1)/2} \times \left[1 + (i-1)! \sum_{k=1}^{i-1} \frac{(-1)^k}{(2k+1)k!(i-1-k)!}\right]\right\}. \quad (8)$$

If $m \leqslant 5$, equation (8) reduces to a simple form

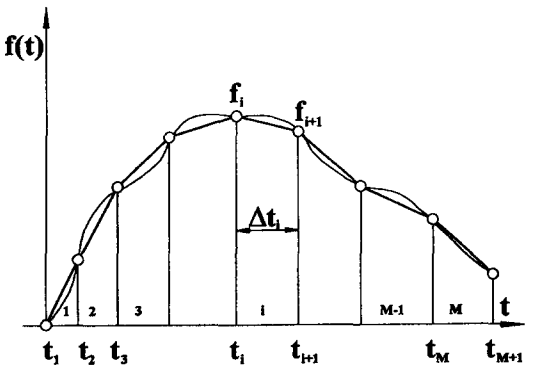

Fig. 3. Piecewise linear interpolation of the time-temperature data.

$$q_E(t) = 2\sqrt{\frac{c_2\rho_2 k_2}{\pi}}[A_1 t^{1/2} + \tfrac{4}{3}A_2 t^{3/2} + \tfrac{8}{5}A_3 t^{5/2} + \tfrac{64}{35}A_4 t^{7/2} + \tfrac{128}{63}A_5 t^{9/2}]. \quad (9)$$

The solutions (6) and (8) have several practical limitations.

Since the inverse solutions given by equation (4) and (5) require continuous first- and high-order derivatives of temperature data $y(t)$ and heat flux q_E, equation (6) is not appropriate. A major weakness of equation (8) is then low accuracy of the polynomial fitting.

Polynomial smoothing allows the calculation of high-order derivatives, but may not reproduce the real data points, especially when the time spread of the fitted data is large.

These restrictions can be avoided by using an alternate procedure based on spline or digital filter smoothing of the temperature–time data.

The experimental temperature is represented by a third-order spline in the form (Fig. 4)

$$y_i(\tau) = C_{1,i} + C_{2,i}(\tau-\tau_i) + \tfrac{1}{2}C_{3,i}(\tau-\tau_i)^2 + \tfrac{1}{6}C_{4,i}(\tau-\tau_i)^3,$$
$$\tau_i \leqslant \tau \leqslant \tau_{i+1}, i = 1, 2, \ldots, M \quad (10)$$

where $\tau = S_t t$ is scaled time and S_t is the scaling factor.

A general cubic polynomial (10) involves four constants:

$$C_{1,i} = y(\tau_i) \neq f(\tau_i),$$
$$C_{2,i} = y'(\tau_i) = \frac{\mathrm{d}y_i(\tau_i)}{\mathrm{d}\tau} = \frac{1}{S_t}\frac{\mathrm{d}y_i(t_i)}{\mathrm{d}t},$$
$$C_{3,i} = y''(\tau_i) = \frac{\mathrm{d}^2 y_i(\tau_i)}{\mathrm{d}\tau^2} = \frac{1}{S_t^2}\frac{\mathrm{d}^2 y_i(t_i)}{\mathrm{d}t^2},$$
$$C_{4,i} = y'''(\tau_i) = \frac{\mathrm{d}^3 y_i(\tau_i)}{\mathrm{d}\tau^3} = \frac{1}{S_t^3}\frac{\mathrm{d}^3 y_i(t_i)}{\mathrm{d}t^3}. \quad (11)$$

There is a sufficient flexibility in the cubic spline approximation to ensure that not only is the smoothing spline continuously differentiable on the interval, but also that it has a continuous second derivative on the interval.

The identical form (10) has the orthogonal Gram polynomial of degree 3 used to construct a digital filter. However, the digital filters do not ensure the continuity of the functions $y_i(\tau)$ and their derivatives at the nodes τ_i.

Starting with equation (2) and the assumption that the surface temperature response is approximated by cubic splines (10), the surface heat flux $q_E(\tau)$ can be expressed as

$$q(\tau_{M+1}) = \left[\sqrt{\frac{c_2\rho_2 k_2}{\pi}}\sum_{i=1}^{M}\int_{\tau_i}^{\tau_{i+1}}\frac{\mathrm{d}y_i(\Theta)}{\mathrm{d}\Theta}\frac{1}{\sqrt{\tau-\Theta}}\mathrm{d}\Theta\right]\sqrt{S_t}$$
$$= \left\{2\sqrt{\frac{c_2\rho_2 k_2}{\pi}}\sum_{i=1}^{M-1}\left[V_i(P_i^{1/2} - R_i^{1/2}) - \frac{W_i}{3}(P_i^{3/2} - R_i^{3/2}) + \frac{C_{4i}}{10}(P_i^{5/2} - R_i^{5/2})\right]\right.$$
$$\left. + 2\sqrt{\frac{c_2\rho_2 k_2}{\pi}}\left(V_M P_M^{1/2} - \frac{W_M}{3}P_M^{3/2} + \frac{C_{4,M}}{10}P_M^{5/2}\right)\right\}\sqrt{S_t},$$
$$M = 1, 2, 3, \ldots, (J-1) \quad (12)$$

where

$$P_i = \tau_{M+1} - \tau_i.$$

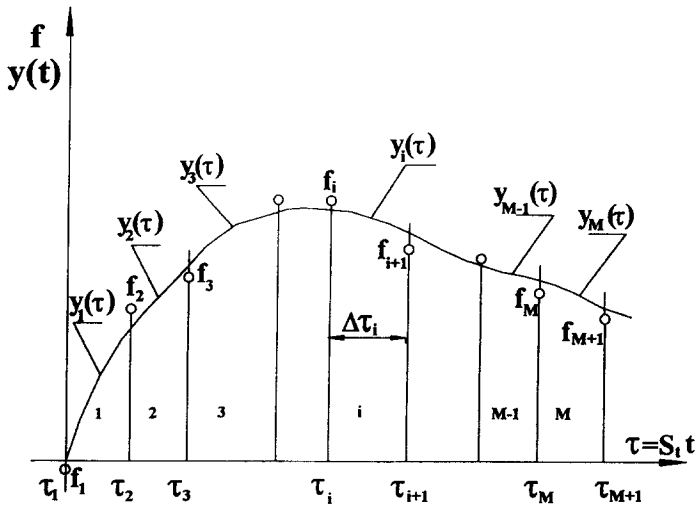

Fig. 4. Cubic spline interpolation of the time-temperature data.

$$R_i = \tau_{M+1} - \tau_{i+1},$$

$$F_i = C_{1,i} + C_{2,i}P_i + \frac{C_{3,i}}{2}P_i^2 + \frac{C_{4,i}}{6}P_i^3,$$

$$V_i = \frac{dF_i}{d\tau_{M+1}} = C_{2,i} + C_{3,i}P_i + \frac{C_{4,i}}{2}P_i^2,$$

$$W_i = \frac{d^2F_i}{d\tau_{M+1}^2} = C_{3,i} + C_{4,i}P_i. \tag{13}$$

The time derivatives required in the exact solutions (4) and (5) can be calculated analytically with high accuracy.

The first two derivatives are

$$\frac{dy_M(t_{M+1})}{dt} = S_t \frac{dy_M(\tau_{M+1})}{d\tau} = S_t V_M,$$

$$\frac{d^2y_M(t_{M+1})}{dt^2} = S_t^2 W_M,$$

$$\frac{dq_E(t_{M+1})}{dt} = S_t \frac{dq_E(\tau_{M+1})}{d\tau}$$

$$= \left\{2\sqrt{\frac{c_2\rho_2 k_2}{\pi}} \sum_{i=1}^{M-1} \left[\frac{V_i}{2}(P_i^{(-1/2)} - R_i^{(-1/2)}) + \frac{W_i}{2}(P_i^{1/2} - R_i^{1/2}) - \frac{C_{4,i}}{12}(P_i^{3/2} - R_i^{3/2})\right] + 2\sqrt{\frac{c_2\rho_2 k_2}{\pi}}\left(\frac{V_M}{2}P_M^{(-1/2)} + \frac{W_M}{2}P_M^{1/2} - \frac{C_{4,M}}{12}P_M^{3/2}\right)\right\} S_t^{3/2}, \quad M = 1, 2, 3, \ldots$$

$$\frac{d^2q_E(t_{M+1})}{dt^2} = S_t^2 \frac{d^2q_E(\tau_{M+1})}{d\tau^2}$$

$$= \left\{2\sqrt{\frac{c_2\rho_2 k_2}{\pi}} \sum_{i=1}^{M-1} \left[-\frac{V_i}{4}(P_i^{(-3/2)} - R_i^{(-3/2)}) + \frac{3W_i}{4}(P_i^{(-1/2)} - R_i^{(-1/2)}) + \tfrac{3}{8}C_{4,i}(P_i^{1/2} - R_i^{1/2})\right] + 2\sqrt{\frac{c_2\rho_2 k_2}{\pi}}\left(-\frac{V_M}{4}P_M^{(-3/2)} + \frac{3W_M}{4}P_M^{(-1/2)} + \tfrac{3}{8}C_{4,M}P_M^{1/2}\right)\right\} S_t^{5/2}, \quad M = 1, 2, 3, \ldots, (J-1). \tag{14}$$

CUBIC SPLINE SMOOTHING OF THE MEASUREMENT DATA

An observation of the time-temperature curve reveals, that small segments of the curve can be closely approximated by cubic splines, equation (10). A spline is simply a piecewise polynomial, the pieces joined together at points called 'knots'. In particular, a cubic spline (10) is a piecewise cubic polynomial, constructed in such a way that second derivative continuity is preserved at the knots. The temperature data are known to be in error. Suppose that pairs of temperature data values (f_i, t_i), $i = 1, \ldots, J$ are observed, and we wish to describe the relationship between them with a regression model

$$f_i = y(t_i) + e \cdot \varepsilon_i, \tag{15}$$

where ε_i are the uncorrelated errors with zero mean and $y(t)$ is the smoothing polynomial spline of degree 3. The total number of measurements is $J > 4$. The more frequently used method of fitting smoothing splines parallels the least squares curve-fitting procedure, by minimizing a criterion that depends on a least-squares-like term, plus a term penalizing roughness. A measure of the rapid local variation of a curve can be given by a roughness penalty such as the integrated squared second derivative. The fitted spline is the solution to the optimization problem [21–25].

Minimize

$$\sum_{i=1}^{J} w_i[y(\tau_i) - f_i]^2 + \lambda \int_{\tau_1}^{\tau_J} [y''(\tau)]^2 \, d\tau, \tag{16}$$

where the parameter $\lambda > 0$ controls the amount of smoothing. If λ is too small, the spline will overfit in the limiting case as $\lambda \to 0$, becoming an interpolating spline. As $\lambda \to \infty$, the smoothing term dominates and removes not only noise, but 'signal' as well. The correct choice of λ is of considerable importance. The method of cross-validation for choosing λ has also been offered as an option for choosing λ [26, 27]. It can be shown [23, 24] that the curve y has the following properties:

(i) is a cubic polynomial in each interval $[\tau_i, \tau_{i+1}]$;

(ii) at the measurement point τ_i, the curve and its first two derivatives are continuous, but there may be a discontinuity in the third derivative.

Schönberg [22] and also Reinsch [23, 24] point out that the spline solution $y(\tau)$ to equation (16) has the property that it minimizes

$$\int_{\tau_1}^{\tau_J} [y''(\tau)]^2 \, d\tau \tag{17}$$

subject to

$$\sum_{i=1}^{J} w_i[y(\tau_i) - f_i]^2 \leqslant S, \tag{18}$$

where S is a given nonnegative number which controls the extent of smoothing.

This, of course, is a global method, requiring all the data points be available before fitting can begin. The choice of the spline smoothing parameter, S, is somewhat arbitrary. Fortunately, a wide optimum range for the smoothing parameter, S, can be found that

gives accurate results. The results obtained for various S differ only in degree of smoothing [28].

If the smoothing parameter, S, is too small, the developed method produces a noise in the estimated surface heat flux or heat transfer coefficient.

The noise error can usually be distinguished from true fluctuation in transient heat transfer without *a priori* knowledge of the noise error with the input signal.

Furthermore, the inverse heat conduction problem involves the calculation of the surface heat flux and heat transfer coefficient from the transient, measured temperature history inside a solid. The higher frequency components of the boundary conditions are damped at an interior point at a higher rate than the lower frequency components. In the inverse heat conduction problem, the boundary conditions are estimated based on the low frequency components of the input signal.

The spline smoothing technique or digital low-pass filtering used in the paper allow us to separate the lower frequency components of the true signal from the higher frequency components in the measurement errors.

For practical purposes, it is sufficient to choose the smoothing parameter S subjectively, by plotting out a few temperature–time curves and choosing the one which 'eliminates best' the high frequency measurement errors from the input data.

If the method developed is to be used routinely on a large number of data sets or a part of a larger procedure then an automatic choice of the smoothing parameter, S, is essential. In these cases the smoothing of the temperature data can be performed using the spline smoothing methods presented in refs. [29, 30]. Both these methods attempt to follow trends in the data and are applicable even if the magnitude of error is unknown. The methods do not require explicit specification of the control parameters. However, the test calculations show, that the method by Reinsch [23] gives more accurate results. If the time steps $\Delta t_i = t_{i+1} - t_i$ are too small or too large it often happens that the minimizing procedure for estimating the spline coefficients becomes ill-conditioned. One way to overcome this difficulty is to introduce scaled time $\tau = S_t t$. The effect of bad scaling in the Reinsch method [23, 24] is that values of spline coefficients: $C_{1,i}, \ldots, C_{4,i}$ are affected by round-off-errors and the sum of squares

$$\sum_{i=1}^{J} w_i [y(\tau_i) - f_i]^2$$

is not equal to the *a priori* given value S.

DIGITAL FILTERING OF MEASUREMENT DATA

The smoothing procedure described above is a global method that requires knowledge of all the data points before construction of the approximating splines can begin. However, for on-line systems, it is frequently necessary to follow and fit the data without knowing its end beforehand. The local method, in which the polynomial pieces are calculated as the data is gathered, is useful for such cases. In the case of a local method, the approximating cubic spline in any interval between data points depends only on a small set of neighbouring data points. For example, an N-point moving digital filter is a local approximation. The digital filter approach is important because it is much more computationally efficient than other methods. Heat transfer coefficient measuring devices can incorporate the digital filter, and immediate graphical output can be provided.

Numerical experiments indicate that for equally spaced data points $7 \leqslant N \leqslant 11$ is satisfactory. Least-squares fitting with orthogonal Gram polynomial of degree 3–11 ($N = 11$) equally spaced data points (Fig. 5) yields for the center point i

$$\begin{aligned}
Y_i = y(t_i) &= \tfrac{1}{429}(-36f_{i-5} + 9f_{i-4} + 44f_{i-3} + 69f_{i-2} \\
&\quad + 84f_{i-1} + 89f_i + 84f_{i+1} + 69f_{i+2} + 44f_{i+3} \\
&\quad + 9f_{i+4} - 36f_{i+5}) \\
Y_i' = \frac{\mathrm{d}y(t_i)}{\mathrm{d}t} &= \frac{1}{5148 \cdot \Delta t}(300f_{i-5} - 294f_{i-4} - 532f_{i-3} \\
&\quad - 503f_{i-2} - 296f_{i-1} + 296f_{i+1} + 503f_{i+2} \\
&\quad + 532f_{i+3} + 294f_{i+4} - 300f_{i+5}) \\
Y_i'' = \frac{\mathrm{d}^2 y(t_i)}{\mathrm{d}t^2} &= \frac{5}{143 \cdot (\Delta t)^2}(f_{i-5} + \tfrac{2}{5}f_{i-4} - \tfrac{1}{15}f_{i-3} \\
&\quad - \tfrac{2}{5}f_{i-2} - \tfrac{3}{5}f_{i-1} - \tfrac{2}{3}f_i - \tfrac{3}{5}f_{i+1} - \tfrac{2}{5}f_{i+2} \\
&\quad - \tfrac{1}{15}f_{i+3} + \tfrac{2}{5}f_{i+4} + f_{i+5}) \\
Y_i''' = \frac{\mathrm{d}^3 y(t_i)}{\mathrm{d}t^3} &= \frac{5}{143 \cdot (\Delta t)^3}(-f_{i-5} + \tfrac{1}{5}f_{i-4} \\
&\quad + \tfrac{11}{15}f_{i-3} + \tfrac{23}{30}f_{i-2} + \tfrac{7}{15}f_{i-1} - \tfrac{7}{15}f_{i+1} - \tfrac{23}{30}f_{i+2} \\
&\quad - \tfrac{11}{15}f_{i+3} - \tfrac{1}{5}f_{i+4} + f_{i+5}).
\end{aligned} \tag{19}$$

Substituting equation (19) into equation (11) gives the coefficients of the spline function (10).

In order to treat each data point in the same manner, the scanning (gathering) of the data should start at least $(N-1)/2 = 5$ time steps Δt before the cooling or heating process starts.

If this is done, the heat flux $q_E(t)$ can be calculated at $t = 0$.

APPLICATION OF PROCEDURES

In order to examine the accuracy of the proposed procedures, three different test cases are solved.

In the first example surface temperature measurements are used to estimate the instantaneous heat flux to a semi-infinite body.

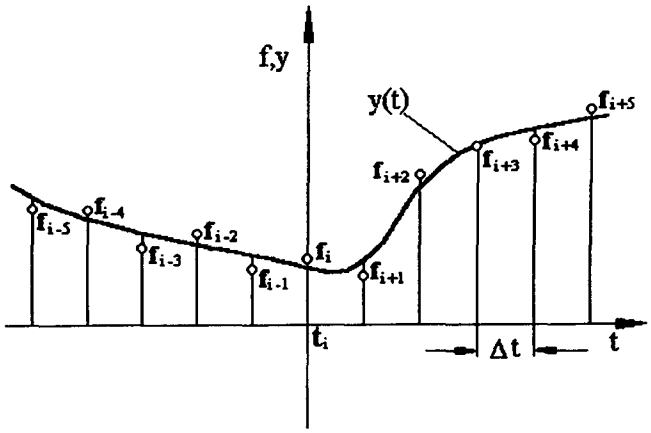

Fig. 5. Digital filtering of the time-temperature data.

A semi-infinite copper body is exposed to the heat flux that varies in time in a triangular fashion

$$q_e(t) = q_{max}\frac{t}{D}, \quad 0 \leqslant \frac{t}{D} \leqslant a;$$

$$q_e(t) = q_{max}\left(1 - \frac{\frac{t}{D}-a}{1-a}\right), \quad a \leqslant \frac{t}{D} \leqslant 1, \qquad (20)$$

where D is heating duration. The maximum heat flux q_{max} occurs at a. The surface temperature history of a semi-infinite solid initially at the uniform temperature $T_0 = 0°C$ is given by ref. [31]

$$T_w = T|_{x=0} = q_{max}\sqrt{\frac{D}{\pi kc\rho}}\frac{4}{3a}\left(\frac{t}{D}\right)^{3/2}, \quad 0 \leqslant \frac{t}{D} \leqslant a,$$

$$T_w = T|_{x=0} = q_{max}\sqrt{\frac{D}{\pi kc\rho}}\frac{4}{3a} \times \left[\left(\frac{t}{D}\right)^{3/2} - \frac{\left(\frac{t}{D}-a\right)^{3/2}}{1-a}\right], a \leqslant \frac{t}{D} \leqslant 1. \qquad (21)$$

The 'measured' temperatures at the surface are simulated by adding a random error ε_j to exact temperatures T_j

$$f_j = T_j + e \cdot \varepsilon_j, j = 1, \ldots, J \qquad (22)$$

where ε_j is a random variable of a uniform distribution with values in the range $[-1, 1]$ and e is the maximum magnitude of the temperature error.

This artificial data is then input into the inverse algorithm and its output is compared to the original assumed heat flux.

Figure 6 shows the artificial data for a particular case $a = 0.5$, $D = 0.1$ s, $q_{max} = 100000$ kW m^{-2}, $T_0 = 0°C$, $kc\rho = 1372.7$ (kJ^2 m^{-4} K^{-2} s^{-1}), $e = 5$ K.

The simulated measured temperature data f_i, containing measurement errors, are shown as the data points in the figure, while the solid line represents the exact data. The time step Δt is $1.4286 \cdot 10^{-3}$ s. There are then 70 time steps ($J = 71$). The dotted line represents the results of measured data smoothing with cubic splines and the parameter values $S_t = 100$ and $S = 434$ K^2.

This value of S was subjectively adjusted. The resulting splines for the temperature data taken at $x = 0$, shown in Fig. 6, give a very good compromise between smoothness and exactness of fit.

A measure of the errors in the temperature measurements $f(t)$ is the sample root mean square norm. It is given by

$$\sigma_f = \sqrt{\frac{1}{J}\sum_{i=1}^{J}[f_i - T_w(t_i)]^2} = e\sqrt{\frac{1}{J}\sum_{i=1}^{J}\varepsilon_i^2}. \qquad (23)$$

In this test case: $\sigma_f = 2.783$ K.

If the discretized computed heat flux component is denoted $q(t_i)$ and the true component is $q_e(t_i)$, in order to measure the error, the root mean square norm is determined as

$$\sigma_q = \sqrt{\frac{1}{J-1}\sum_{i=2}^{J}[q(t_i) - q_e(t_i)]^2}. \qquad (24)$$

In this equation the summation is from $i = 2$ as $q(t = 0)$ is not known.

Some numerical results for errorless measurements with $\sigma_f = 0$ and inexact measurement with $\sigma_f = 2.783$ K are shown in Figs. 7 and 8. Figure 7 shows the results for errorless data. Clearly, the agreement between the estimated and the true heat flux is excellent.

The spline smoothing approach to interpolating temperature measurements produces better results than the interpolation by straight-line pieces, the difference is not large though. The root mean squared errors in q are $\sigma_{q,l} = 190.3$ kW m^{-2} and $\sigma_{q,s} = 70.7$ kW m^{-2} for piecewise linear and spline interpolation, respectively.

The results obtained by using measurements with

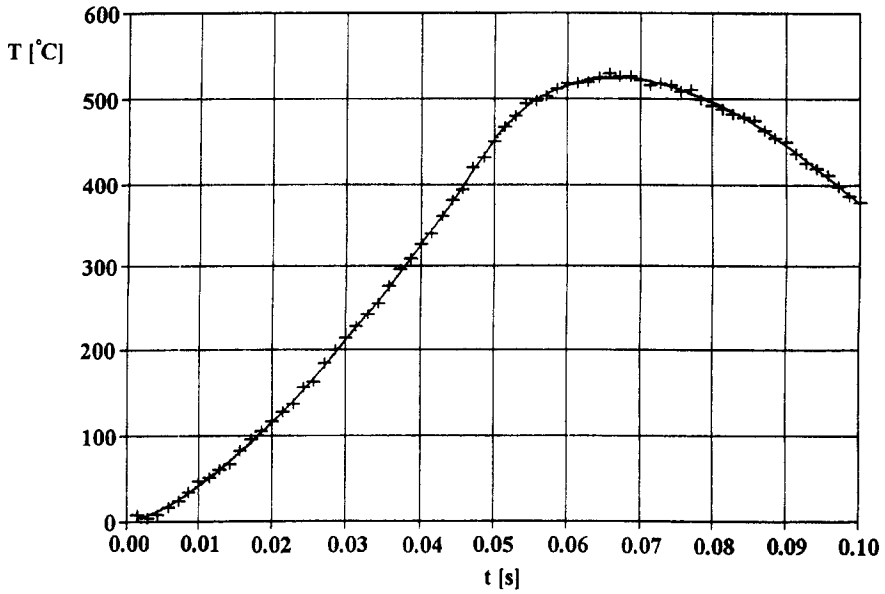

Fig. 6. Surface temperature of semi-infinite body for triangular heat flux; —— errorless temperature measurements, +—inexact temperature measurements.

random errors are also in good agreement with the exact (known) heat flux history, in spite of large errors in the input data (Fig. 8). The spline interpolation, in conjunction with Duhamel's integral method, yields results slightly better than more common piecewise linear interpolation ($\sigma_{q,s} = 3096.5$ kW m^{-2} and $\sigma_{q,l} = 3577$ kW m^{-2}).

However, the interpolation of the input data has limited applicability because the estimated heat flux curve is noisy and time derivatives of the surface heat flux $q_e(t)$ cannot be evaluated with sufficient accuracy. When a spline smoothing technique with $S = 434$ K^2 is applied to the inexact temperature–time data, excellent results are again obtained.

Figure 9 shows that the triangular shape of heat flux is quite well reproduced and the results are smooth. The root mean squared error is $\sigma_{q,s} = 935.1$ kW m^{-2}. The results of the application of the three techniques for calculating the surface heat flux clearly indicate that the spline smoothing technique is superior to the piecewise linear and spline interpolation procedures.

In the second example a transient technique for measuring heat transfer between a flowing fluid and a solid surface is presented.

In the experiments, whereas a high temperature surface was spray cooling with water spray, the heat transfer coefficient is evaluated from the transient

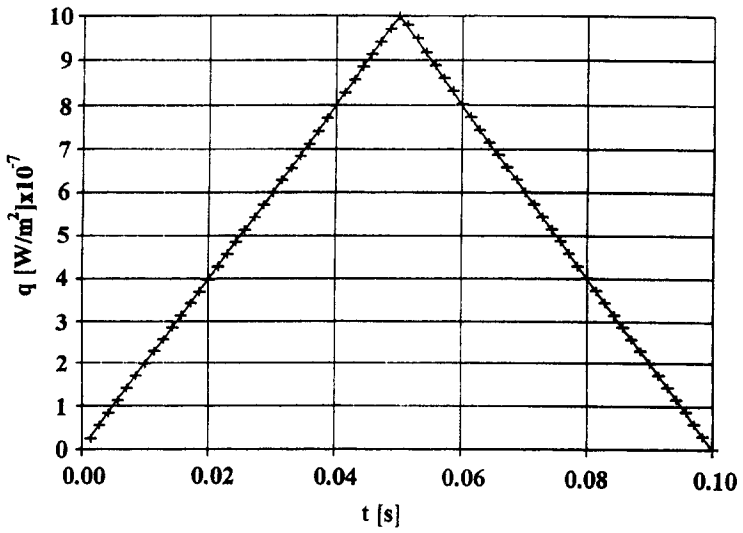

Fig. 7. Calculated surface heat flux with errorless data; —— known (exact) heat flux and calculated heat flux for spline interpolation of the time-temperature data, +—calculated heat flux—piecewise linear interpolation of the time-temperature data.

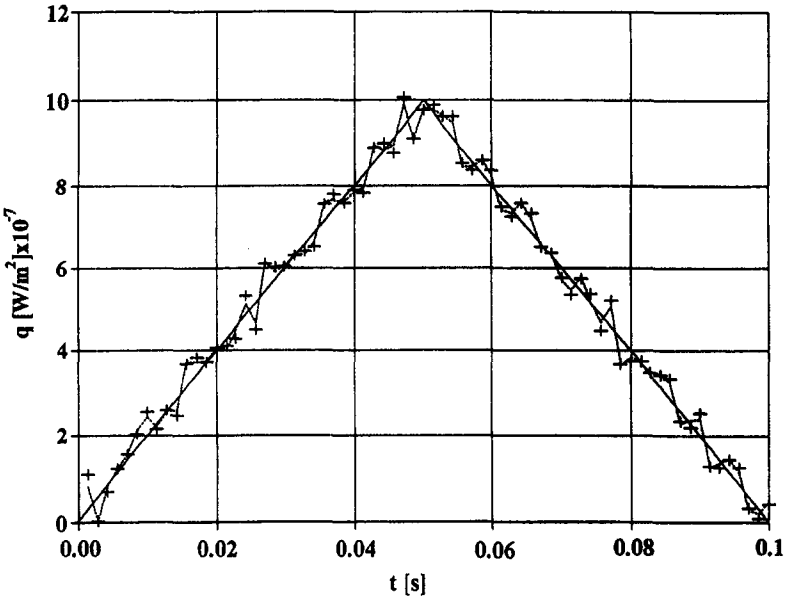

Fig. 8. Calculated surface heat flux for inexact temperature data; —— known (exact) heat flux, +— piecewise linear interpolation of the time-temperature data, – – – –spline interpolation of the time-temperature data.

response of the solid at some interior point $x = E$. When the solid has a low thermal diffusivity and is very thick or when the transient of interest is very short, the solid temperature response is limited to a thin layer near the surface and the solid may be considered to be a semi-infinite medium.

In order to test the accuracy of the method, approximate recovering of heat transfer coefficient $h(t)$ is investigated for semi-infinite solid, initially heated to a uniform temperature T_0 and suddenly exposed to convective environment. The heat transfer coefficient h and fluid temperature T_∞ are assumed constant over the duration of the experiment. The exact data for this problem are generated using the analytical solution [1] given by

$$T(x,t) = T_\infty + (T_0 - T_\infty)\{erf\xi + \exp(Bi+\eta) \cdot [1 - erf(\xi + \sqrt{\eta})]\}, x \geqslant 0, \quad (25)$$

where

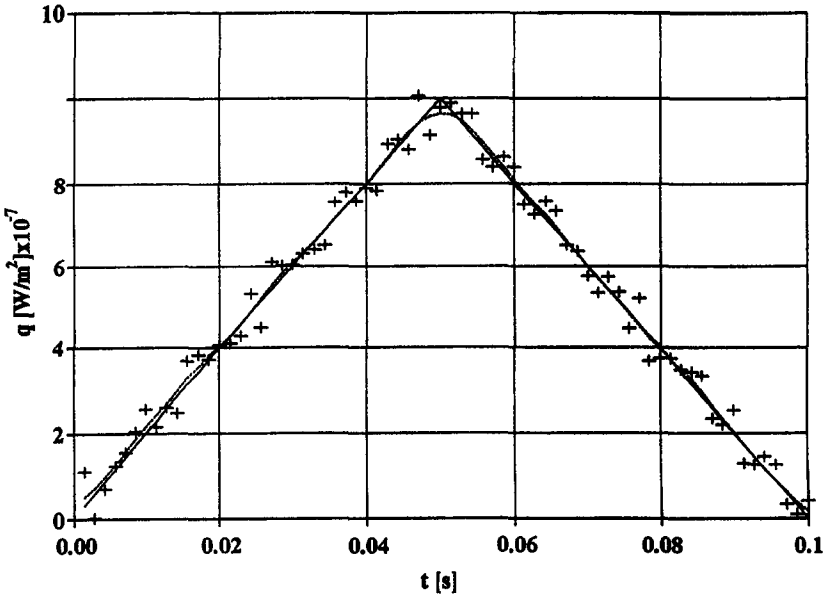

Fig. 9. Calculated surface heat flux for inexact temperature data; —— known (exact) heat flux, +— piecewise linear interpolation of the time-temperature data, – – – –spline approximation of the time-temperature data ($S = 434\ K^2$).

$$\xi = \frac{x}{2\sqrt{\alpha t}},$$

$$Bi = \frac{h \cdot x}{k},$$

$$\eta = \frac{h^2 \cdot t}{c\rho k}.$$

The exact surface heat flux is then calculated as follows:

$$q_s = q(0,t) = -k\left.\frac{\partial T}{\partial x}\right|_{x=0} = h[T_\infty - T_s(t)], \quad (26)$$

where the surface temperature is obtained from equation (25); the result is

$$T_s(t) = T(0,t) = T_\infty + (T_0 - T_\infty) \times \exp(\eta) \cdot [1 - erf(\sqrt{\eta})]. \quad (27)$$

The transient heat flux at $x = E$ is calculated using the equation (12).

The temperature field and the surface heat flux are determined using the exact solution (4) and (5).

Only two first terms in equations (4) and (5) were evaluated to compute the temperature and heat flux responses with a good accuracy.

The 'measured' temperatures are obtained from equation (22) for $e = 2$ K. Simulated experimental temperatures have been generated for 101 time points with a time step of 1 s. The root mean squared error in the temperature data is $\sigma_T = 1.147$ K.

A temperature sensor is located at an interior point, $E = 0.006$ m below the cooled surface. The thermal properties of the test body (a thick steel wall of the PWR reactor) are assumed to be constant and the following values are used: $k = 42$ W m^{-1} K^{-1}, $\alpha = 11.6 \cdot 10^{-6}$ m^2 s^{-1}, $c\rho k = 158\,629\,212$ J^2 m^{-4} K^{-2} s^{-1}.

Figure 10 shows the exact (solid line) and simulated measured temperatures (crosses) for the parameters values: $h = 2000$ W m^{-2} K, $T_0 = 300$°C, $T_\infty = 20$°C.

The effect of inaccuracies in the measurement of the interior temperature is minimized by smoothing the raw interior temperature–time data prior to the calculation of the heat transfer coefficient.

The spline smoothing approach with $S_t = 1$ and $S = 150$ K^2 or the 11-point digital filter ($N = 11$) are used to smooth the corrupted data.

For this value of smoothing parameter, S, the curve $y(t)$ in Fig. 12 looks very good, i.e. is smooth and eliminates random errors.

The fluid temperature $T_\infty = 20$°C is not disturbed by random errors.

When a third-order spline interpolation ($S = 0$) is applied to the disturbed temperature–time data of Fig. 10, the results are of little interest because the estimation of the heat transfer coefficient is very poor. Therefore, graphical results for this case are not presented.

Notice that though h is actually constant, it is determined as though it were a time varying function $h(t)$.

The root mean square norm for h is determined as

$$\sigma_h = \sqrt{\frac{1}{J-1}\sum_{i=2}^{J}[h(t_i) - h_e(t_i)]^2}, \quad (28)$$

where $h(t_i)$ is the computed heat transfer coefficient and $h_e(t_i)$ is the true value of $h(t)$ at t_i.

Figure 10 shows the calculated temperature at the surface ($x = 0$) and at the location $x = E/2 = 0.003$ m for the errorless data ($S_T = 0, S = 0$). Clearly, the agreement between the estimated and the exact surface temperature is excellent. The true surface temperature is indicated by empty squares. Figure 11 depicts the estimated heat flux at $x = E = 0.006$ m and at the

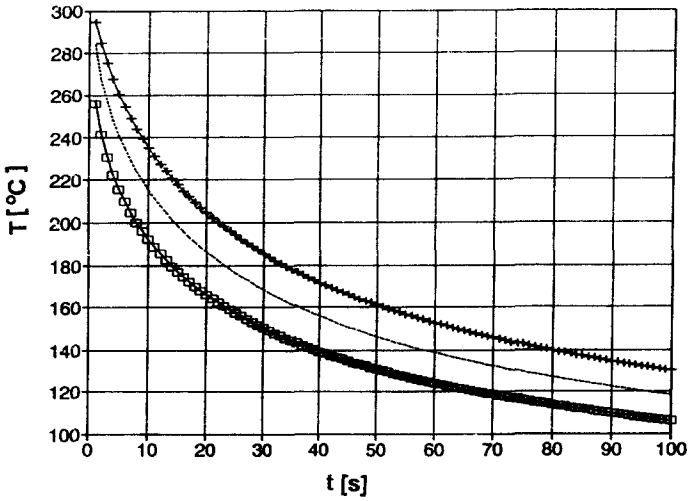

Fig. 10. Temperature of a semi-infinite body determined from temperature measurements at the location $x = E = 0.006$ m, using spline approximation of the temperature-data; +—exact data, ···—spline interpolation ($S = 0$), – – – –calculated temperature at $x = E/2 = 0.003$ m, ——calculated surface temperature, □—exact surface temperature.

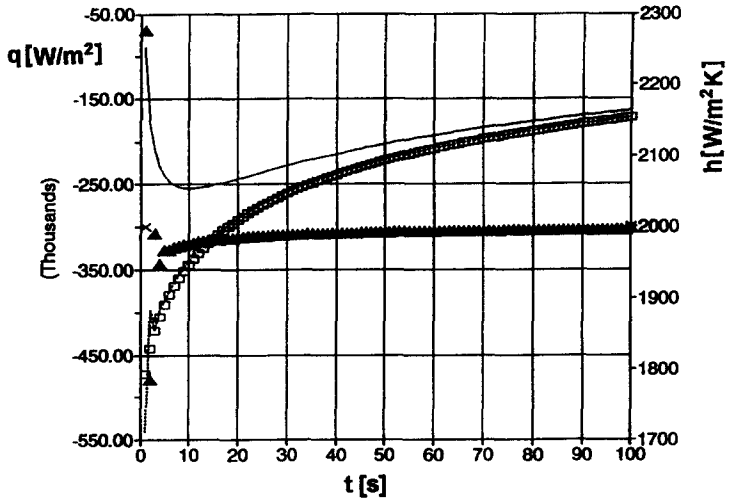

Fig. 11. Heat transfer coefficient and surface heat flux determined from exact temperature data at $x = E = 0.006$ m using spline approximation ($S = 0$) of the temperature; · · ·—heat flux at $x = E = 0.006$ m, – – – –surface heat flux, □—exact surface heat flux, ▲—heat transfer coefficient.

surface ($x = 0$), and the heat transfer coefficient for the same data used in Fig. 10. The root mean squared error in h for $\sigma_f = 0$ is: $\sigma_h = 37.6\ \mathrm{W\ m^{-2}\ K^{-1}}$. Inspection of Figs. 10 and 11 indicates that both the true surface heat flux and temperature are in very good agreement, although some oscillations in the heat transfer coefficient are observed near $t = 0$. The estimated surface heat flux and heat transfer coefficient exhibit greater errors associated with lower accuracy of the spline smoothing for a short time. In addition, to achieve higher accuracy, the third- and higher-order derivatives should be retained in the series (5) as $t \to 0$.

The effect of the uncertainty in the input temperature data can be seen in Figs. 12 and 13. Note that the temperature measurement errors primarily affect the estimated heat transfer coefficient ($\sigma_h = 95\ \mathrm{W\ m^{-2}\ K^{-1}}$). Compared to the error in the recovered heat flux and heat transfer coefficient, the calculated temperatures are found to be less sensitive to random errors in the data. It should be noted that prior to applying the inverse heat conduction procedure, the temperature–time data have been smoothed using the cubic spline with $S = 150\ \mathrm{K^2}$.

When the 11-point digital filter is applied to the same disturbed temperature–time data, the results (Figs. 14 and 15) are in fair agreement with the true values ($\sigma_h = 143.1\ \mathrm{W\ m^{-2}\ K^{-1}}$). For the case of

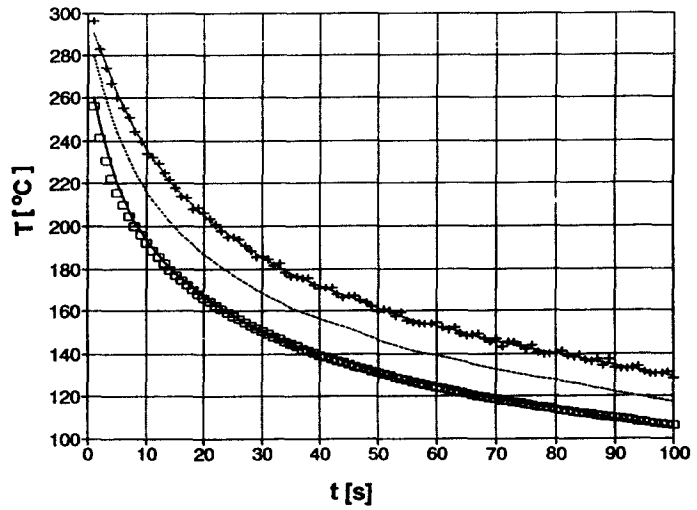

Fig. 12. Temperature of semi-infinite body determined from inexact temperature measurements at the location $x = E = 0.006$ m using spline approximation of the temperature data; +—inexact temperature data, · · ·—spline approximation ($S = 150\ \mathrm{K^2}$), – – – –calculated temperature at $x = E/2 = 0.003$ m, ——calculated surface temperature, □—exact surface temperature.

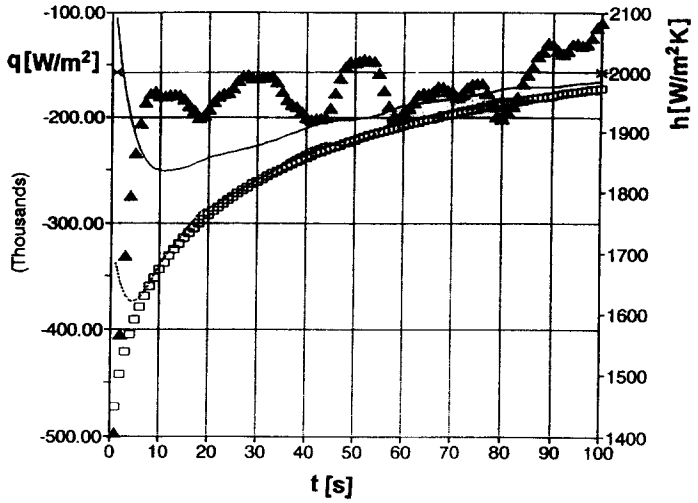

Fig. 13. Heat transfer coefficient and surface heat flux determined from inexact temperature measurements at the location $x = E = 0.006$ m using spline approximation of the temperature data; ···—heat flux at $x = E = 0.006$ m, – – – –surface heat flux, □—exact surface heat flux, ▲—heat transfer coefficient.

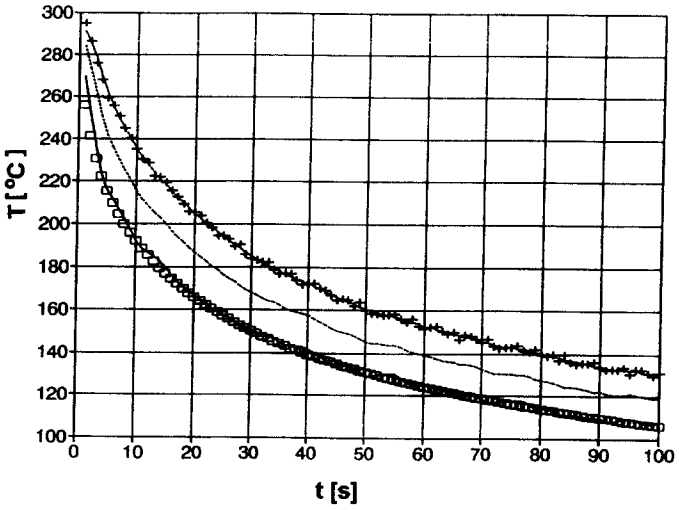

Fig. 14. Temperature of semi-infinite body determined from inexact temperature measurements at the location $x = E = 0.006$ m using the 11-point digital filter for smoothing of the temperature data; + — inexact temperature data, ··· —smoothed temperature using the 11-point digital filter, – – –calculated temperature at $x = E/2 = 0.003$ m, — calculated surface temperature, □—exact surface temperature.

$\sigma_f = 1.147$ K, the results look good, but not as smooth as those for the spline smoothing approach. The scatter in the estimated heat flux and heat transfer coefficient is caused primarily by the piecewise approximation used in digital filtering. Unlike the smoothing splines, in digital filtering neither the function nor its first derivatives are required to be continuous. If the errors in the time–temperature data are smaller ($e = 0.5$ K, $\sigma_f = 0.287$ K), the resulting heat transfer coefficient is much smoother and gives a very good representation of the true value (Fig. 16) ($\sigma_h = 105.8\,\mathrm{W\,m^{-2}\,K^{-1}}$). The advantage of the digital filter approach is that it requires less computer time, particularly as more time steps are considered.

In the third example, the actual measured data from a thermal shock experiment are considered [32].

The heat transfer to droplets impinging on a heated surface was investigated based on experimentally acquired temperature at an interior location of a semi-infinite body. The rapid cooling of a hot solid surface with an impinging water jet is used in many industrial processes.

Typical applications are found in the continuous casting processes of metallurgical industries and the emergency cooling of pressure vessels of PWR reactors [33].

The experimental study presented in ref. [32] was made in attempting to obtain the fundamental infor-

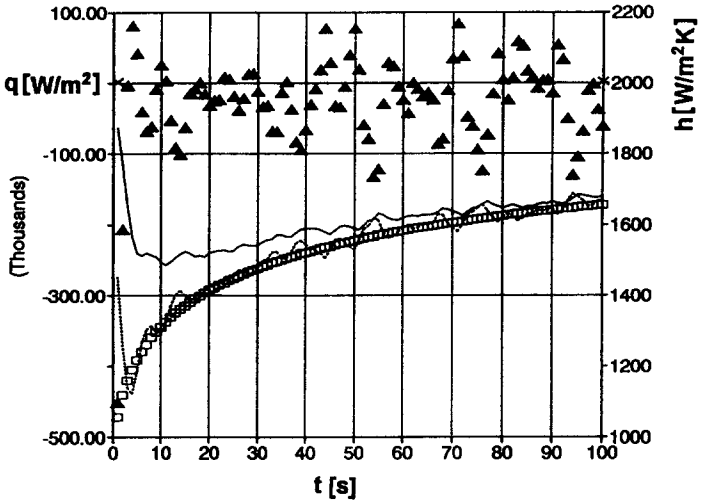

Fig. 15. Heat transfer coefficient and surface heat flux determined from inexact temperature measurements at the location $x = E = 0.006$ m. The temperature data with errors from interval ± 2 K smoothed using the 11-point digital filter; ···—heat flux at $x = E = 0.006$ m, – – – –surface heat flux, □—exact surface heat flux, ▲—heat transfer coefficient.

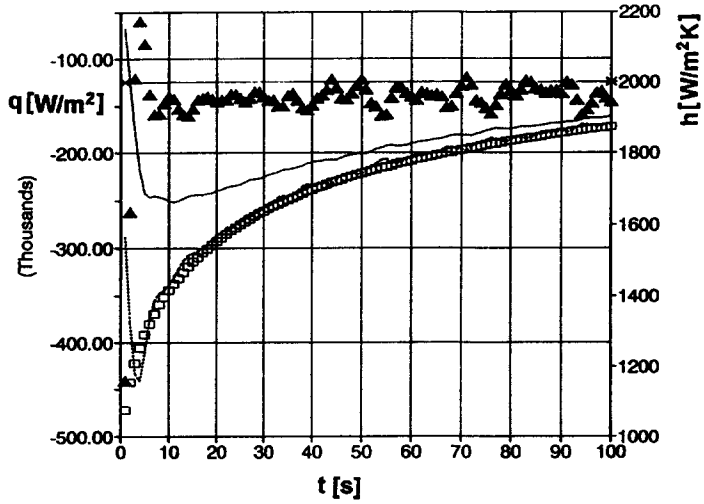

Fig. 16. Heat transfer coefficient and surface heat flux determined from inexact temperature measurements at the location $x = E = 0.006$ m. The temperature data with errors from interval ± 0.5 K smoothed using the 11-point digital filter (nomenclature as Fig. 15).

mation concerning the heat transfer from a heated wall to saturated droplets deposited on it in the post-dryout mist flow regime.

Measurements of the surface heat flux during the residence time of a droplet on the high temperature surface were made based on the time-dependent variation of the wall temperature measured near the surface.

The test surface was a 0.01 m diameter and 0.005 m thick stainless steel disc supported by a sheathed chromel–alumel thermocouple of 0.00065 m O.D located at the centre of the disc. The thermocouple junction is located at distance $E = 0.0003$ m from the cooled surface.

In the present study, the surface temperature and heat flux are calculated from recorded temperature variations at $x = E = 0.0003$ m, assuming that the disc behaves as a semi-infinite body with uniform initial temperature.

The thermal properties of the disc material are assumed to be constant as follows:

$$k = 17.65\,\mathrm{W\,m^{-1}\,K^{-1}},$$

$$\alpha = 4.26 \cdot 10^{-6}\,\mathrm{m^2\,s^{-1}},$$

$$c\rho k = 73127307\,\mathrm{J^2\,m^{-4}\,K^{-2}\,s^{-1}}.$$

The inverse heat conduction (IHC) calculations are performed on the experimental temperature data shown in Table 1.

For these computations, $S_t = 10\,000$ is used. Prior to applying the IHC procedure, the time–temperature

Table 1. Temperature–time variations, measured at a distance of $x = E = 0.0003$ m on droplet impingement

i	t_i [s]	f_i [°C]
1.	0	250.0
2.	0.001	249.8
3.	0.002	249.3
4.	0.003	247.6
5.	0.004	245.3
6.	0.005	242.3
7.	0.006	240.1
8.	0.007	238.0
9.	0.008	236.6
10.	0.009	236.0
11.	0.01	235.5
12.	0.011	235.3
13.	0.012	235.2
14.	0.013	235.25
15.	0.014	235.3
16.	0.015	235.4

data from the thermocouple are approximated by cubic spline functions using the Reinsch method with $S = 0.5\ \mathrm{K}^2$.

In this case, the small value of S was chosen, as the number of data points is not large ($J = 16$) and the temperature measurements $f(t_i)$ (Fig. 17) $i = 1, \ldots, 16$ are not noisy.

Figure 17 shows the temperature decay in a semi-infinite body (stainless steel disc). The surface temperature decreases sharply on the droplet impingement, but its recovery after the droplet rebounding is also rapid. Although the value of $E = 0.0003$ m is small, the temperature difference between the point $x = E$ and the cooled surface: $x = 0$ is large. Also the heat flux at location $x = E$ differs very significantly from that at the surface (Fig. 18). The heat flux at the disc surface changes in a complicated manner with time on droplet impingement. During the direct contact of the impinging droplet with the metal surface, the surface heat flux decreases remarkably. Then, the surface temperature increases and the state shifts to film boiling—a spheroidal state—with a thin steam film between the droplet and disc surface. The heat transfer rate to the droplet in a spheroidal state is very low [32]. Positive surface heat flux in the time interval $6.5\ \mathrm{s} < t < 12\ \mathrm{s}$ results probably from errors of the temperature measurements at $x = E = 0.0003$ m. Using the method developed, the transient surface heat transfer to the droplets impinging on a heated surface can be examined in detail.

CONCLUDING REMARKS

A technique for determining the transient heat flux and heat transfer coefficient at a solid interface, based on experimentally acquired interior temperature–time data, is developed. For the analysed case of a single interior temperature history, the problem is subdivided into two separate problems: a direct problem for the semi-infinite solid and an inverse problem for the flat plate. The heat flux at the location of the temperature sensor is determined from the solution of one-dimensional heat conduction using Duhamel's theorem. Global and local spline approximations are used to smooth the measured interior temperature–time curves. A general case closed form equation for the interface heat flux is obtained.

Knowing both the temperature and heat flux at a sensor location, the temperature and heat flux at the active surface are determined from the solution of the inverse heat conduction problem using Stefan–Burggraf–Langford method.

The total and global cubic spline approximations of the measured temperature data are compared for the same test cases. The methods generally give a similar answer, but the global spline approximation gives slightly better results, e.g. more accurate and

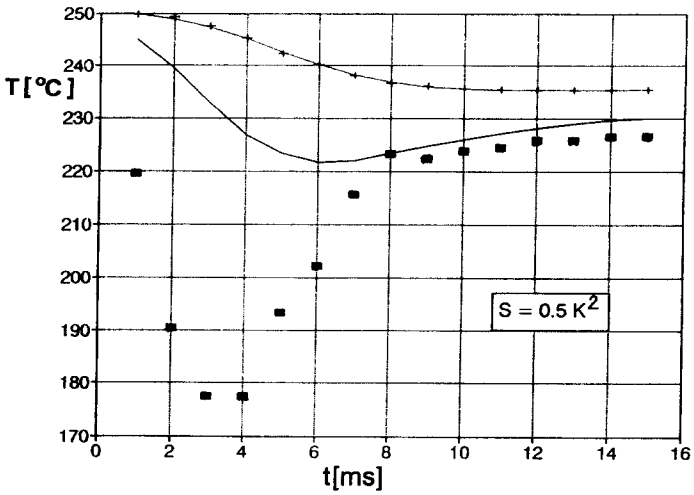

Fig. 17. Cooling curves of semi-infinite body after the impingement of saturated droplets upon a heated surface; +—temperature data at $x = E = 0.0003$ m, ···—spline approximation of the temperature data ($S = 0.5\ \mathrm{K}^2$), — — calculated temperature at $x = E/2 = 0.00015$ m, ■—calculated surface temperature.

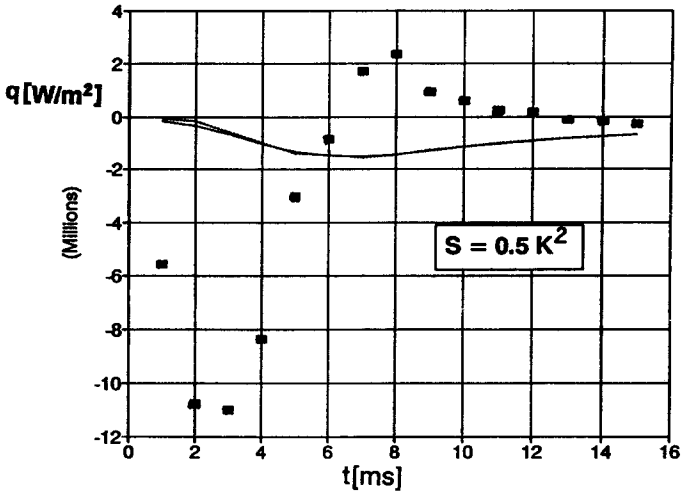

Fig. 18. Heat flux results after the impingement of saturated droplets upon a heated surface; – – – –heat flux at $x = E = 0.0003$ m determined by using piecewise linear interpolation of the temperature data, · · · · heat flux at $x = E = 0.0003$ m determined by using spline approximation of the temperature data ($S = 0.5$ K^2), ■ —surface heat flux determined by using spline approximation of the temperature data.

smoother. In terms of computing time, the local spline approximation takes much less time than the global approximation. The local approximation has the advantage that the inverse heat conduction problem can be solved on-line on a personal computer.

The developed technique is also very useful for handling very complex geometries. Clearly, it is not precise to use equation (2) as the formula for calculating the transient heat transfer coefficient for non-planar boundaries, but for short duration experiments, the heat conduction within the solid can be assumed to be locally one-dimensional, neglecting the heat flow along the boundary surface. The local, time-dependent heat transfer coefficients can be determined from measured temperature–time variations at several subsurface points of the solid. This technique has the following advantages:

(1) it is economical because a short duration test does not require much time to carry out the experiment;

(2) the measurements can be obtained with simple, low cost experimental models and equipment;

(3) although the data analysis is relatively complicated, the computing time is very small.

REFERENCES

1. H. S. Carslaw and J. C. Jaeger, *Conduction of Heat in Solids*. Clarendon Press, Oxford (1959).
2. W. J. Cook and E. J. Felderman, Reduction of data from thin-film heat-transfer gauges; a concise numerical technique, *AIAA J.* **4,** 561–562 (1966).
3. H. Consigny and B. E. Richards, Short duration measurements of heat-transfer rate to a gas turbine rotor blade, *ASME J. Engng Power* **104,** 542–551 (1982).
4. D. M. Kercher, R. E. Sheer, Jr and R. M. C. So, Short duration heat transfer studies at high free-stream temperatures, *ASME J. Engng Power* **105,** 156–166 (1983).
5. Ch. G. Miller, Refinement of an "alternate" method for measuring heating rates in hypersonic wind tunnels, *AIAA J.* **23,** 810–812 (1985).
6. J. E. Doorly and M. L. G. Oldfield, The theory of advanced multi-layer thin film heat transfer gauges, *Int. J. Heat Mass Transfer* **30,** 1159–1168 (1987).
7. P. R. A. Lyons and S. L. Gai, A method for the accurate determination of the thermal product $(\rho ck)^{1/2}$ for thin film heat transfer or surface thermocouples gauges, *J. Phys. E: Sci. Instrum.* **21,** 445–448 (1988).
8. A. H. George and J. L. Smalley, An instrumented cylinder for the measurement of instantaneous local heat flux in high temperature fluidized beds, *Int. J. Heat Mass Transfer* **34,** 3025–3036 (199?).
9. J. W. Baughn, P. T. Ireland, T. V. Jones and N. Saniei, A comparison of the transient and heated-coating methods for the measurement of local heat transfer coefficients on a pin fin, *ASME J. Heat Transfer* **111,** 877–881 (1989).
10. S. A. Hippensteele and P. E. Poinsatte, Transient liquid-crystal technique used to produce high-resolution convective heat-transfer-coefficient maps, HTD-Vol. 252, *Visualization of Heat Transfer Processes*. ASME, New York (1993).
11. T. E. Diller and D. P. Telionis, Time-resolved heat transfer and skin friction measurements in unsteady flow. In *Advances in Fluid Mechanics Measurement* (Edited by M. Gad-el-Hak), pp. 323–355. Springer, New York (1989).
12. W. D. Harvey, Instrumenting models for aerodynamic heat transfer studies involving transient heating rates. *ISA Trans.* **6,** 42–46 (1967).
13. T. V. Jones, Heat transfer, skin friction, total temperature and concentration measurements. In *Measurement in Heat Transfer* (Edited by E. R. G. Eckert and R. J. Goldstein), pp. 63–102. Hemisphere–McGraw-Hill, New York (1977).
14. C. T. Kidd, Thin-skin technique heat-transfer measurement errors due to heat conduction into thermocouple wires. *ISA Trans.* **24,** 1–9 (1985).
15. C. T. Kidd, Lateral heat conduction effects on heat-transfer measurements with the thin-skin technique. *ISA Trans* **26,** 7–18 (1987).
16. R. C. Mehta, T. Jayachandran and V. M. K. Sastri, Finite element analysis of conductive and radiative heating of a thin skin calorimeter. *Wärme Stoffübertragung* **22,** 227–230 (1988).
17. J. Stefan, Über die Theorie der Eisbildung insbesondere über Eisbildung im Polarmeere. Sitzungsberichte der Kaiserlichen Akademie Wiss. *Wien, Math. Natur.* **98,** 965–983 (1889).

18. O. R. Burggraf, An exact solution of the inverse problem in heat conduction theory and applications. *ASME J. Heat Transfer* **86C,** 373–382 (1964).
19. D. Langford, New analytic solutions of the one-dimensional heat equation for temperature and heat flow rate both prescribed at the same fixed boundary (with applications to the phase change problem). *Q. Appl. Math.* **24,** 315–322 (1967).
20. J. Taler and W. Zima, Measurement of time-varying heat transfer coefficient. *Inżynieria Chem. Procesowa* (*Chem. Process Engng*) **4,** 535–554 (1993) (in Polish).
21. E. J. Wegman and I. W. Wright, Spline in statistics, *J. Am. Statist. Ass.* **78,** 351–365 (1983).
22. I. J. Schoenberg, Spline functions and the problem of graduation, *Proc. Natl Acad. Sci. U.S.A.* **52,** 947–950 (1964).
23. C. H. Reinsch, Smoothing by spline functions I, *Numer. Math.* **10,** 177–183 (1967).
24. C. H. Reinsch, Smoothing by spline functions II, *Numer. Math.* **16,** 451–454 (1971).
25. C. de Boor, *A Practical Guide to Splines.* Springer, New York (1978).
26. P. Craven and G. Wahba, Smoothing noisy data with spline functions: estimating the correct degree of smoothing by the method of generalized cross-validation, *Numer. Math.* **31,** 377–403 (1979).
27. G. Wahba, How to smooth curves and surfaces with splines and cross-validation, *Proceedings of the 24th Conference on the Design of Experiments*, U.S. Army Research Office, Report 79-2 (1979).
28. J. Taler, Numerical solutions for general inverse heat conduction problem. *Wärme Stoffübertragung* **27,** 505–513 (1992).
29. M. J. D. Powell, Subroutine VC03, Harwell Subroutine Library. Computer Science and Systems Division, Harwell Subroutine Library. Computer Science and Systems Division, Harwell Laboratory, Oxfordshire, England (1985).
30. K. Ichida and T. Kiyono, Curve fitting by a one-pass method with a piecewise cubic polynomial. *ACM Trans. Matl Software* **3,** 164–174 (1977).
31. P. J. Schneider, Conduction. In *Handbook of Heat Transfer* (Edited by W. M. Rohsenow and J. P. Hartnett), Section 3. McGraw-Hill, New York (1973).
32. T. Ueda, T. Enomoto and M. Kanetsuki, Heat transfer characteristics and dynamic behavior of saturated droplets impinging on heated vertical surface, *Bull. JSME* **22,** 724–732 (1979).
33. J. Taler, Notkühlsimulation der Reaktordruckbehälter von Druckwasserreaktoren. Forschungsheft der Technischen Universität Kraków, Nr. 151, pp. 1–123, Kraków (1993).